Evidence of scattering of tropospheric radiation by PSCs in mid-IR limb emission spectra: MIPAS-B observations and KOPRA simulations

M. Höpfner, H. Oelhaf, G. Wetzel, F. Friedl-Vallon, A. Kleinert, A. Lengel, G. Maucher, H. Nordmeyer, N. Glatthor, G. Stiller, T. v. Clarmann, H. Fischer

Institut für Meteorologie und Klimaforschung, Forschungszentrum Karlsruhe, Germany

C. Kröger, T. Deshler

Department of Atmospheric Science, University of Wyoming, Laramie, USA

Abstract. Polar stratospheric clouds (PSCs) were observed by the high resolution mid infrared Michelson Interferometer for Passive Atmospheric Sounding, Balloon borne version (MIPAS-B), on a flight from Kiruna/Sweden on January 11, 2001. Highly resolved spectral features in the limb measurements could only be explained by tropospheric radiation scattered into the line of sight by large PSC particles. Furthermore, model calculations showed that for PSCs with particles of radius ≥ 1 μm a significant part of the broadband continuum radiance signal is due to scattering. Inclusion of scattering in the retrieval process resulted in reasonable values of otherwise largely overestimated PSC volume density profiles.

1. Introduction

Mid infrared remote sensing of stratospheric sulfate aerosols and polar stratospheric clouds (PSCs) has been used to derive information on composition, volume and size parameters. Many of these observations were solar absorption measurements from the ground [*Höpfner et al.*, 2001], from aircraft [*Kinne et al.*, 1989] or from satellite [*Rinsland et al.*, 1994; *Eldering et al.*, 2001; *Hervig et al.*, 1998]. Limb emission experiments probing stratospheric aerosols include balloon observations described by *Halperin and Murcray* [1987], the Michelson Interferometer for Passive Atmospheric Sounding, Balloon borne version (MIPAS-B) [*Echle et al.*, 1998], as well as three satellite instruments: the Improved Stratospheric And Mesospheric Sounder (ISAMS) [*Lambert et al.*, 1996], the Cryogenic Limb Array Etalon Spectrometer (CLAES) [*Massie et al.*, 1996], and the Cryogenic Spectrometers and Telescopes for the Atmosphere (CRISTA) [*Spang et al.*, 2001].

While absorption measurements provide extinction coefficients more directly, the primary output of emission instruments are radiance spectra. From these, aerosol extinction coefficient profiles are retrieved on the basis of radiative transfer calculations. Subsequently, the extinctions are used to derive aerosol parameters [*Grainger et al.*, 1995; *Massie et al.*, 1998]. Such a stepwise approach requires a retrieval of extinction coefficients independent of aerosol properties. This approach fails if scattering effects, largely depending on particle radius, have a significant impact on the simulated radiance. In previous work scattering was often neglected under the assumption that particles are small and thus absorption is predominant in comparison to scattering [*Lambert et al.*, 1996; *Massie et al.*, 1996]. To overcome this problem *Echle et al.* [1998] developed an iterative scheme to correct extinction coefficients by use of low resolution forward model calculations including scattering.

It was shown by *Halperin and Murcray* [1987] that for certain aerosol size distributions a significant contribution of the measured limb radiance originates from layers below the tangent point and from the earth's surface. Furthermore, there are indications that retrieved limb emission extinction coefficients are sometimes too large compared with absorption measurements or in-situ aerosol profiles [*Hervig and Deshler*, 1998; *Massie et al.*, 1998; *Lambert et al.*, 1996]. Neglect of scattered background radiance would explain the overestimation since in this case the retrieval can reproduce the measured radiation only by enhanced emission of aerosols.

In the following we will demonstrate, by use of unprecedented high resolution broadband limb emission measurements of synoptic PSCs by MIPAS-B together with radiative transfer simulations, that radiation scattered into the line of sight must be taken into account to correctly explain limb radiance observations in the presence of PSCs.

2. MIPAS-B experiment and observations

MIPAS-B is a balloon borne limb viewing interferometer with an unapodized spectral resolution of 0.034 cm^{-1}. It covers the mid infrared region from 770–1950 cm^{-1} in four spectra channels [*Fischer and Oelhaf*, 1996; *Friedl-Vallon et al.*, 1999].

During a flight on January 11, 2001 from Kiruna (Sweden, 67.8°N/20.4°E) limb emission spectra were recorded in northward and southward directions from a floating level of about 28.5 km. Tangent altitudes ranged from around 10 km up to flight level. All measurements were located inside the stratospheric polar vortex. Tangent point temperatures in northward direction were up to 7 K lower than those along the southward views. Figure 1 compares northward spectra with southward spectra for a tangent altitude of 20.3 km. The strongly increased broadband continuum signal of the northward spectrum is evidence for PSCs in the line of sight which are not present in the southward observations. Apart from this radiance offset further characteristic PSC features are (1) a steplike spectral signature between 815 and 825 cm^{-1}, (2) sidelobes of CO_2 lines, and (3) inverted H_2O lines (expanded view box in Figure 1).

3. Data analysis and results

3.1. Radiative transfer model

The Karlsruhe Optimized and Precise Radiative transfer Algorithm (KOPRA) was used as basis for profile retrievals and broadband line by line radiative transfer simulations [*Stiller et al.*, 2002].

Copyright by the American Geophysical Union.

Paper number .
0094-8276/01/$5.00

To simulate aerosol effects and to support aerosol parameter retrieval KOPRA includes an aerosol model based on Mie theory. This model provides aerosol absorption and scattering cross sections and phase functions as well as the derivatives of these variables with respect to aerosol size parameters and refractive indices [*Höpfner and Echle*, 2000]. Altitude dependent mono- ($M = 1$) and bi- ($M = 2$) modal lognormal particle size distributions defined by number densities ($N_i(h)$), median radii ($r_i(h)$) and mode widths ($s_i(h)$) are supported:

$$n(r,h) = \sum_{i=1}^{M} \frac{N_i(h)}{r s_i(h)\sqrt{2\pi}} \exp\left[-\frac{\ln^2(r/r_i(h))}{2 s_i(h)^2}\right], \qquad (1)$$

where r is the particle radius and h the altitude.

The inclusion of a Mie model into the forward code offers the possibility to retrieve aerosol parameters directly from the measured radiances, i.e. the above mentioned stepwise procedure does not have to be used. Thus, effects of scattering can properly be taken into account during the retrieval.

The radiative transfer part of KOPRA includes the following processes: (1) absorption by molecules and aerosols, (2) aerosol scattering out of the line of sight, (3) emission by molecules and aerosols, (4) single aerosol scattering of terrestrial and (5) of solar radiation into the line of sight. Since the MIPAS-B measurements were performed during night process (5) had not to be considered for the following analysis.

3.2. Retrieval scenarios

For comparison with the measured radiances between 800 and 1300 cm^{-1}, four aerosol scenarios (SC1–SC4) were considered. In all cases, first, a retrieval of vertical profiles of total PSC number density ($N(h) = N_1(h) + N_2(h)$) was performed in narrow spectral windows based on the full set of measured limb spectra. Using the result of $N(h)$, in a second step, broadband forward model calculations including and neglecting scattering of tropospheric radiation into the line of sight were made for 20.3 km tangent altitude. SC1 includes only the small particle mode of the baseline PSC size distribution as described below. SC2 includes both the small and large mode. To improve the comparison, SC3, which increases the second mode median radius and width, and SC4, which is SC3 with a tropospheric cloud, were also tried. An overview of these scenarios is given in Table 1, and comparisons of the results with the measurements are shown in Figure 2 and Figure 3.

Common for all scenarios were the spectral windows, temperature and trace gas profiles, and profiles of aerosol refractive indices. As spectral windows we chose the following regions with low trace gas continuum interference: 827–829 cm^{-1}, 947–950 cm^{-1}, and 1210–1214 cm^{-1}. For temperature and HNO_3 we used profiles which were retrieved from the northward measurements under consideration of the best possible aerosol parameter fits. To test this temperature profile we also used ECMWF analyses which can directly be fed into KOPRA in a 3-dimensional radiative transfer mode. Resulting differences in retrieved number densities were negligible. The volume mixing ratio profile for H_2O was a combination of a retrieval result from the southward limb scan for the lower stratosphere and sonde profiles for the troposphere. Information about the composition of the PSCs, which determines the refractive indices to be used, were derived from co-located measurements performed the day after the MIPAS-B flight. Backscatter sonde data from balloons launched from Kiruna [*Larsen*, private communication] and Sondankylä [*Kivi et al.*, 2001], as well as airborne LIDAR data [*Flentje*, private communication] agree in suggesting that most of the PSCs were spherical droplets commonly thought to consist of sulfuric ternary $H_2O/H_2SO_4/HNO_3$ solution (STS). Therefore, we used equilibrium calculations to determine the composition of STS droplets with altitude [*Carslaw et al.*, 1995]. As input for these calculations HNO_3 and H_2O profiles from retrievals of the southward views and the temperature profile fit for the northward spectra were used. H_2SO_4 was set to 0.5 ppbv. In the region of the PSCs (19–26 km) the STS equilibrium composition ranged from 50 wt % H_2SO_4, 3 wt % HNO_3 (19 km) to 3 wt % H_2SO_4, 43 wt % HNO_3 (21–24 km) and back to 45 wt % H_2SO_4, 6 wt % HNO_3 (26 km). From the composition profiles and the atmospheric temperature, KOPRA internally determines wavenumber dependent refractive indices of STS using the scheme of *Biermann et al.* [2000] to feed the Mie model.

As a baseline for PSC size distributions, particle counter measurements from the January 12 balloon flight were taken. In the region between 19 and 26 km a smoothed altitude dependent bimodal distribution was derived with minimum–maximum values of r_1 = 0.15–0.21 μm, s_1 = 0.38–0.57, r_2 = 0.8–1.2 μm, s_2 = 0.11–0.15, and $N_1/(N_1 + N_2)$ = 0.96–0.99.

3.3. Results

For scenario SC1 only the small particle mode 1 was used to retrieve number density. From the resulting $N(h)$ and the fixed size parameters the total aerosol volume density was derived and plotted in Figure 2 in comparison with volume density derived from the particle counter measurements on January 12 and equilibrium STS calculations for January 11. Obviously the retrieved volume on the basis of only small particles is much larger than measured in situ as well as calculated for STS equilibrium conditions as described in the previous section.

Based on the retrieved number density profile, broadband forward calculations for the tangent altitude of 20.3 km were performed and compared with the measured radiances. Figure 3 shows the result of these simulations for complete radiative transfer and for a case where the scattered radiance into the line of sight was neglected. It is obvious for SC1 that (1) the calculated broadband continuum around 950 cm^{-1} is too small in comparison with the result at 830 or 1200 cm^{-1}, (2) the simulated spectral signature between 800 and 840 cm^{-1}, which is due to the ν_2 band of NO_3^-, does not fit the measured sharp step at 820 cm^{-1}, (3) there are no sidelobes of CO_2 lines or inversed H_2O lines in the simulation, and (4) the difference of the continua calculated with and without scattering into the line of sight is negligible for longer wavelengths and increases up to 14% at 1200 cm^{-1}.

SC2 included both, the small as well as the large particle mode of the particle counter measurements. Figure 3 shows that the CO_2 line sidelobes and inversed H_2O lines now appear in the simulated spectrum which includes scattering. The explanation for this effect is that the larger particles of the second mode much more effectively scatter the tropospheric radiance spectrum into the line of sight. Due to the warm background of the earth's surface the tropospheric signal is an absorption type spectrum. Thus, the sidelobes of the CO_2 lines are due to superposition of pressure broadened tropospheric absorption lines with stratospheric emission lines. Because of the large tropospheric H_2O content the weak stratospheric water signatures are totally dominated by the strong absorption signal of the scattered spectrum. Furthermore, the broadband continuum is strongly increased by the scattered radiance. The fraction of scattered to total radiance ranges from 16% at 800 cm^{-1} to 40% at 1200 cm^{-1}. The effect of the scattered radiance continuum contribution on the retrieval is a decrease of the aerosol volume density compared to SC1 (Figure 2). The values for SC2, however, are still larger than the in situ measurements and the STS equilibrium calculations.

Owing to this discrepancy and because the modelled CO_2 sidelobes in SC2 were not strong enough, the radius and width of the second mode were increased to r_2 = 2 μm and s_2 = 0.3. The effect of this change, called SC3, on the simulated spectra is rather strong (see Figure 3). While the H_2O signatures are now much larger than the measured ones, the CO_2 sidelobes fit quite well. The scattered radiance makes up to 85% of the total continuum at 1200 cm^{-1}. This leads to a further decrease of the volume density profile to values which are comparable to the in situ measurements and the STS equilibrium calculations (Figure 2).

The large influence of scattered radiation on limb spectra in the presence of PSCs implicates a dependence on the actual tropospheric situation. In SC4 this impact was analyzed by adding a tropospheric cloud as grey body with an optical depth of 0.3 at 8 km altitude to scenario SC3. Due to the absorption of the signal from atmospheric layers below the cloud the inversed H_2O lines are attenuated and become comparable to those of the measurement (Figure 3). However, the CO_2 sidelobes are now slightly smaller than observed. Furthermore, the lower surface temperature of the cloud compared to the earth's surface reduces the scattered contribution to the broadband signal. Thus, the retrieved volume density increases, but it still remains reasonable (see Figure 2). The broadband continuum structure of SC4 fits better to the measurements than in all previous scenarios. However, the simulated radiance is still too low around 950 cm^{-1}.

4. Conclusions

It was demonstrated that highly resolved spectral features in MIPAS-B limb emission spectra of PSCs were due to scattering of tropospheric radiation by particles larger than 1 μm radius. Furthermore, in the presence of such particles a considerable part of the continuum radiance is caused by scattering. Therefore, reasonable number densities only can be retrieved if scattering of tropospheric radiation is taken into account. This has implications on those aerosol and PSC parameter retrievals which are based on extinction data derived from limb emission sounders without taking scattering into account. We have solved this problem by implementing a Mie model and calculating single scattering into the line of sight within the forward code KOPRA. Thus, the retrieval of altitude dependent aerosol parameters directly from the radiance spectra is possible.

Retrieval is complicated by the strong impact of tropospheric conditions on the measured radiance. Future work might introduce the tropospheric cloud cover as a further parameter to be determined and might use as many tropospheric information as possible from independent sources. Remaining discrepancies in the analysis of MIPAS-B PSC observations are the steplike feature around 820 cm^{-1}, which appears only as a much broader signal in the simulation, as well as higher measured radiances in the 950 cm^{-1} region. These differences could be caused by inaccurate laboratory data of refractive indices or by a different composition of the PSCs. However, retrievals with refractive index data for various other kinds of PSCs resulted in worse fits between measured and simulated radiances compared to STS.

For future missions of limb emission instruments, like MIPAS on ENVISAT, it is important to realize that more information on particle size can be gained by investigating the highly resolved spectral features than just by considering broad scale continuum structures. This will be of interest for the detection of very large PSC particles which have been discovered recently [*Fahey et al.*, 2001].

Acknowledgments. The work presented in this paper was supported within the German AFO-2000 programme (BMBF grant 07ATF04). We are grateful to the CNES launching team and the staff of the SSC Esrange for the excellent balloon operations and logistical support as well as the ECMWF for providing us meteorological data via NILU. We thank H. Flentje from DLR and N. Larsen from DMI for provision of unpublished data.

References

Biermann, U.M., B.P. Luo, Th. Peter, Absorption spectra and optical constants of binary and ternary solutions of H_2SO_4, HNO_3, and H_2O in the mid infrared at atmospheric temperatures, *J. Phys. Chem. (A), 104*, 783–793, 2000.

Carslaw, K.S., B.P. Luo, and Th. Peter, An analytic expression for the composition of aqueous HNO_3–H_2SO_4 stratospheric aerosols including gas phase removal of HNO_3, *Geophys. Res. Lett., 22*, 14, 1877–1880, 1995.

Echle, G., T. von Clarmann, H. Oelhaf, Optical and microphysical parameters of the Mt. Pinatubo aerosol as determined from MIPAS-B mid-IR limb emission spectra, *J. Geophys. Res., 103*, D15, 19193–19211, 1998.

Eldering, A., F.W. Irion, A.Y. Chang, M.R. Gunson, F.P. Mills, H.M. Steele, Vertical profiles of aerosol volume from high-spectral resolution infrared transmission measurements. I. Methodology, *Appl. Opt., 40*, 18, 3082–3091, 2001.

Fahey, D.W., et al., The detection of large HNO_3-containing particles in the winter Arctic stratosphere, *Science, 291*, 1026-1031, 2001.

Fischer, H., and H. Oelhaf, Remote sensing of vertical profiles of atmospheric trace constituents with MIPAS limb-emission spectrometers, *Appl. Opt., 35*, 16, 2787-2796, 1996.

Friedl-Vallon, F., G. Maucher, H. Oelhaf, M. Seefeldner, O. Trieschmann, G. Wetzel, H. Fischer, The balloon-borne Michelson Interferometer for Passive Atmospheric Sounding (MIPAS-B2) - Instrument and Results, *Proc. SPIE, 3756*, 9-16, 1999.

Grainger, R.G., A. Lambert, C.D. Rodgers, F.W. Tayler, Stratospheric aerosol effective radius, surface area and volume estimated from infrared measurements, *J. Geophys. Res., 100*, D8, 16507–16518, 1995.

Halperin, B. and D. Murcray, Effect of volcanic aerosol on stratospheric radiance at wavelengths between 8 and 13 μm, *Appl. Opt., 26*, 11, 2222–2235, 1987.

Hervig, M.E., T. Deshler, J.M. Russell III, Aerosol size distributions obtained from HALOE spectral extinction measurements, *J. Geophys. Res., 103*, D1, 1573–1583, 1998.

Hervig, M.E., and T. Deshler, Stratospheric aerosol surface area and volume inferred from HALOE, CLAES, and ILAS measurements, *J. Geophys. Res., 103*, D19, 25345–25352, 1998.

Höpfner, M., and G. Echle, The broadband continuum implementation, in *The Karlsruhe Optimized and Precise Radiative transfer Algorithm (KOPRA), Wissenschaftliche Berichte, FZKA 6487*, edited by G. P. Stiller, pp. 93–98, 2000.

Höpfner, M., T. Blumenstock, F. Hase, A. Zimmermann, H. Flentje, S. Fueglistaler, Mountain polar stratospheric cloud measurements by ground based FTIR solar absorption spectroscopy, *Geophys. Res. Lett., 28*, 11, 2189–2192, 2001.

Kinne, S., O.B. Toon, G.C. Toon, C.B. Farmer, E.V. Browell, M.P. McCormick, Measurements of size and composition of particles in polar stratospheric clouds from infrared solar absorption spectra, *J. Geophys. Res., 94*, D14, 16481–16491, 1989.

Kivi, R., E. Kyrö, A. Dörnbrack, T. Birner, Observations of vertically thick polar stratospheric clouds and record low temperatures in the Arctic vortex, *Geophys. Res. Lett., 28*, 19, 3661–3664, 2001.

Lambert, A., et al., Validation of aerosol measurements from the improved stratospheric and mesospheric sounder, *J. Geophys. Res., 101*, D6, 9811–9830, 1996.

Massie, S.T., et al., Validation studies using multiwavelength Cryogenic Limb Array Etalon Spectrometer (CLAES) observations of stratospheric aerosol, *J. Geophys. Res., 101*, D6, 9757–9773, 1996.

Massie, S.T., D. Baumgardner, J.E. Dye, Estimation of polar stratospheric cloud volume and area densities from UARS, stratospheric aerosol measurement II, and polar ozone and aerosol measurement II extinction data, *J. Geophys. Res., 103*, D5, 5773–5783, 1998.

Rinsland, C.P., G.K. Yue, M.R. Gunson, R. Zander, M.C. Abrams, Mid-infrared extinction by sulfate aerosols from the Mt Pinatubo eruption, *J. Quant. Radiat. Transfer, 52*, 3/4, 241–252, 1994.

Spang, R., M. Riese, D. Offermann, CHRISTA-2 observations of the south polar vortex in winter 1997: A new dataset for polar process studies, *Geophys. Res. Lett., 28*, 16, 3159–3162, 2001.

Stiller, G.P., T. v. Clarmann, B. Funke, N. Glatthor, F. Hase, M. Höpfner, A. Linden, Sensitivity of trace gas abundances retrievals from infrared

limb emission spectra to simplifying approximations in radiative transfer modeling, *J. Quant. Radiat. Transfer, 72*, 3, 249–280, 2002.

M. Höpfner, H. Oelhaf, G. Wetzel, F. Friedl-Vallon, A. Kleinert, A. Lengel, G. Maucher, H. Nordmeyer, N. Glatthor, G. Stiller, T. v. Clarmann, H. Fischer, Institut für Meteorologie und Klimaforschung, Forschungszentrum Karlsruhe, Postfach 3640, D-76021 Karlsruhe, Germany. (michael.hoepfner@imk.fzk.de, hermann.oelhaf@imk.fzk.de)

C. Kröger, T. Deshler, Department of Atmospheric Science, University of Wyoming, Laramie, WY 82071, USA. (ckroger@uwyo.edu, deshler@uwyo.edu)

(Received _____.)

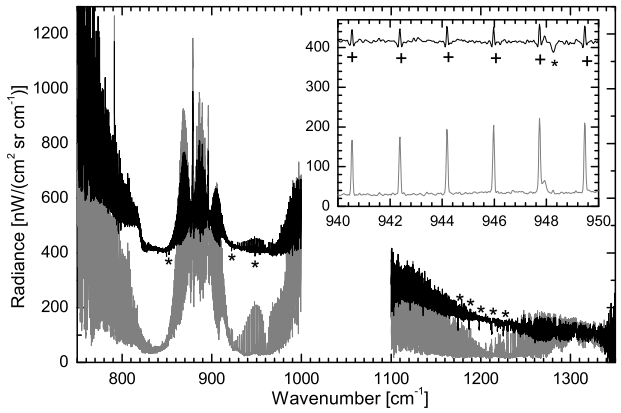

Figure 1. MIPAS-B limb emission spectra (channels 1 and 2) of January 11, 2001 for 20.3 km tangent altitude. Black curve: northward measurement with PSC in the line of sight. Grey curve: southward measurement without evident PSC signal. Examples for CO_2 lines with sidelobes are indicated by (+) and inversed H_2O lines by (*).

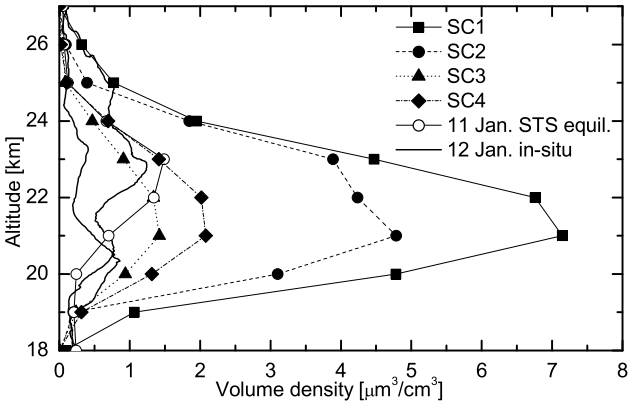

Figure 2. PSC volume density profiles. Filled symbols: retrieved for scenarios SC1–SC4. Open symbols: calculated on basis of STS equilibrium for the retrieved temperature profile from the MIPAS-B northward views. Solid line: smoothed particle counter measurements from January 12, 2001 (larger values during ascent, smaller during descent).

Table 1. Retrieval scenario definition. Intervals are minimum–maximum values in the altitude range 19-26 km.

	SC1	SC2	SC3	SC4
r_1 [μm]	0.15–0.21	0.15–0.21	0.15–0.21	0.15–0.21
s_1	0.38–0.57	0.38–0.57	0.38–0.57	0.38–0.57
r_2 [μm]	-	0.8–1.2	2.0	2.0
s_2	-	0.11–0.15	0.3	0.3
$N_1/(N_1+N_2)$	1	0.96–0.99	0.96–0.99	0.96–0.99
Tropospheric cloud	no	no	no	yes

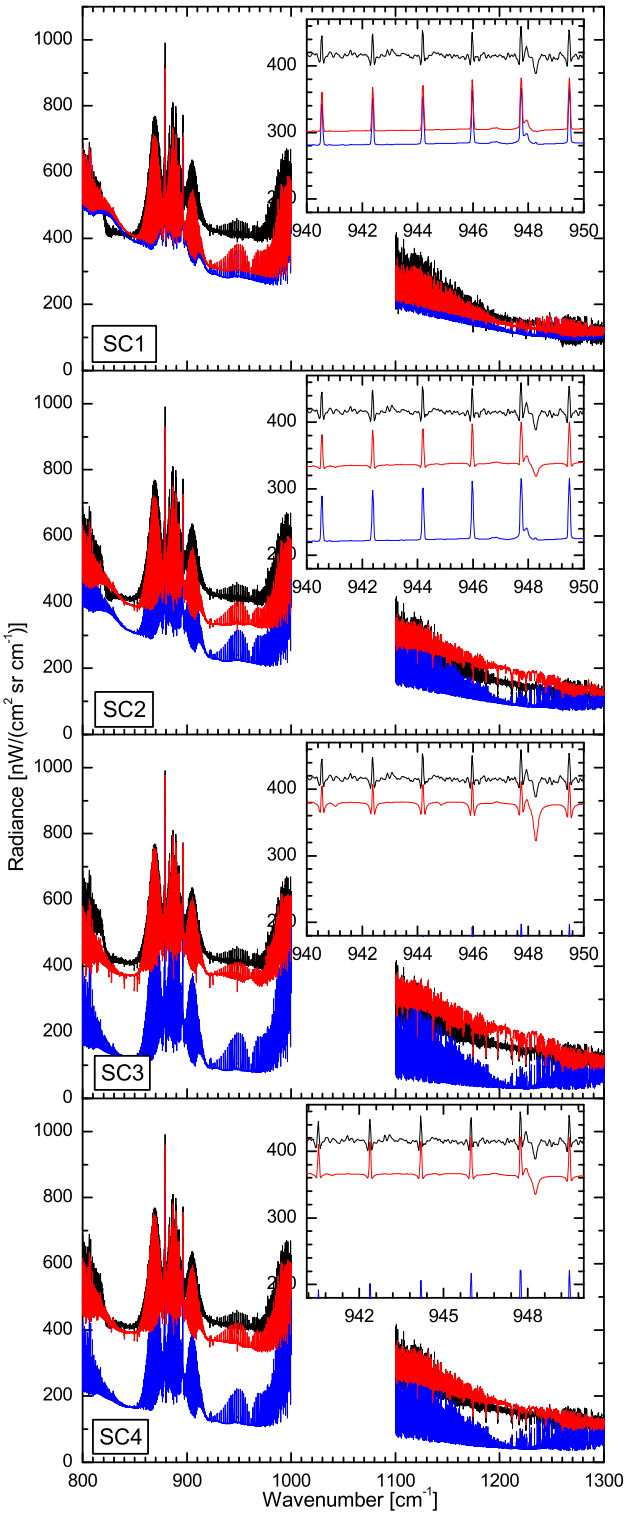

Figure 3. High resolution broadband calculations for the different retrieval scenarios SC1–SC4 compared to the observation (tangent altitude: 20.3 km). The measurement is black, the calculation with scattering into the line of sight is red and the calculation without scattering into the line of sight is blue.